Pergamon

Int. J. Heat Mass Transfer. Vol. 39, No. 16, pp. 3325–3332, 1996

0017–9310/96 $15.00+0.00

PII: S0017-9310(96)00046-4

Radiation affected compressible turbulent flow over a backward facing step

SANG SOO KIM and SEUNG WOOK BAEK†

Korea Advanced Institute of Science and Technology, Aerospace Engineering Department, 373-1 Gusungdong, Yusungku, Taejon, Korea

(*Received* 11 *August* 1995 *and in final form* 12 *January* 1996)

Abstract—A numerical analysis has been conducted to examine combined radiation–convection–conduction heat transfer over a backward facing step flow. The LU-SSOR scheme and finite volume method were used to solve the compressible Navier–Stokes equation and energy equation, while the radiative transfer equation was solved by discrete ordinates method (DOM). The thermal behavior has been influenced such that the fluid was heated up faster due to the radiation. Furthermore, the reattachment length was also shrunk because of the reduced adverse pressure gradient. However, the radiative heat flux was found to play some role in the recirculating zone only. Copyright © 1996 Elsevier Science Ltd.

1. INTRODUCTION

The problem of an absorbing, emitting gas flow in a backward facing step geometry has many engineering applications, such as in industrial furnaces and in a solid fuel ramjet engine. In the design of these high-performance systems it is very important to be able to predict its related thermo-fluid dynamic structure.

A number of analyses with conduction, convection and radiation have been reported in other geometries rather than backward facing step. Kobiyama *et al.* [1] studied the two-dimensional radiative effects on laminar and turbulent flows of purely absorbing gray fluids which pass through a finite heating section with constant wall temperature. Kim and Lee [2] examined a thermally developing Poiseuille flow with anisotropic scattering between two infinite parallel plates. The problem of two-dimensional preheating of a gray fluid in a thermally developing pipe was also investigated by Echigo *et al.* [3]. The combined heat transfer in a tube flow with a finite length was solved by Smith *et al.* [4], while the nongray medium was assumed to be isotropically scattering as well as absorbing.

On the other hand, the work concerning a backward facing step has rarely been reported. Chai *et al.* [5] discussed the effects of radiation in the backward facing step flow, but it was strictly restricted to incompressible laminar flow. In their analysis, the flow field was totally decoupled from the energy field due to the assumption of constant properties. The flow in a solid fuel ramjet combustor, which is accompanied by very high temperature and velocity, must be compressible as well as turbulent [6]. Therefore, the thermo-fluid variables of velocity, pressure, density and temperature are closely coupled with one another. The main objective of this study resides in understanding the effects of radiation on the compressible, turbulent flow in the backward facing step geometry, which has not been done before.

As a numerical algorithm of the compressible Navier–Stokes equation, LU-SSOR (lower–upper symmetric successive over relaxation) implicit scheme is chosen for time differencing, while the finite volume method is adopted for space differencing. The zero-equation algebraic model developed by Baldwin–Lomax is used for modeling the turbulence effect. The radiative transfer equation is analyzed by using the discrete ordinates method (DOM).

2. THEORETICAL MODEL

2.1. *Governing equations*

As schematically shown in Fig. 1, the compressed air at high temperature enters the channel and flows over the backward facing step. Here, $H = 0.0381$ m, $H_1 = 2H$ and the expansion ratio $H_2/H_1 = 1.5$. The computation is carried out on a physical domain beginning 6 step-heights upstream of the step and ending 30 step-heights downstream of the step. The upstream computational domain is not only required to maintain a stable solution near the step, but also to allow the appropriate establishment of inlet condition at the step. In the work, the main objective is to seek the role of radiation in the compressible, turbulent flow. Therefore, a kind of radiatively active gray gases are presumed to be already mixed with the air. However, since their volume fraction is small, their effects on gaseous physical properties are neglected here. In order to simulate the inner environment of a solid fuel ramjet combustor, the step side wall, as well as the bottom wall behind the step, is considered

† Author to whom correspondence should be addressed.

NOMENCLATURE

a	absorption coefficient
e_t	total internal energy
C_p	specific heat at constant pressure
H	step height
I	intensity of radiation
J	Jacobian
p	pressure
q	heat flux
r	radial coordinate
s	scattering coefficient
T	temperature
t	time
u, v	streamwise and transverse velocity components
x, y	Cartesian coordinates.

Greek symbols

λ	thermal conductivity
μ	viscosity
ξ, η	streamwise and transverse computational coordinates
ρ	density
σ	Stefan–Boltzmann constant, 5.67×10^{-8} W (m^2 K^4)$^{-1}$
Φ	scattering phase function
Ω	angular direction.

Superscripts

n	time index.

Subscripts

i, j	grid indices
t	total
w	wall.

to be held at very high temperature, whereas all other walls are assumed to be adiabatic as shown in the figure.

The dimensionless two-dimensional continuity, momentum and energy equations that are used in the analysis can be written in generalized coordinates as follows:

$$\frac{\partial\tilde{\mathbf{Q}}}{\partial t}+\frac{\partial\tilde{\mathbf{F}}}{\partial\xi}+\frac{\partial\tilde{\mathbf{G}}}{\partial\eta}=\frac{\sqrt{\gamma}}{Re}\left(\frac{\partial\tilde{\mathbf{F}}_v}{\partial\xi}+\frac{\partial\tilde{\mathbf{G}}_v}{\partial\eta}\right) \tag{1}$$

where $Re=\rho a_\infty H/\mu$

$$\tilde{\mathbf{Q}}=\frac{1}{J}\begin{bmatrix}\rho\\ \rho u\\ \rho v\\ \rho e_t\end{bmatrix}\quad \tilde{\mathbf{F}}=\frac{1}{J}\begin{bmatrix}\rho U\\ \rho uU+\xi_x p\\ \rho vU+\xi_y p\\ (\rho e_t+p)U\end{bmatrix}$$

$$\tilde{\mathbf{G}}=\frac{1}{J}\begin{bmatrix}\rho V\\ \rho uV+\eta_x p\\ \rho vV+\eta_y p\\ (\rho e_t+p)V\end{bmatrix}, \tag{2}$$

where $U=\xi_x u+\xi_y v$, $V=\eta_x u+\eta_y v$

$$\tilde{\mathbf{F}}_v=\frac{1}{J}(\xi_x\mathbf{F}_v+\xi_y\mathbf{G}_v)\quad \tilde{\mathbf{G}}_v=\frac{1}{J}(\eta_x\mathbf{F}_v+\eta_y\mathbf{G}_v)$$

$$\mathbf{F}_v=\begin{bmatrix}0\\ \tau_{xx}\\ \tau_{xy}\\ u\tau_{xx}+v\tau_{xy}-q_x\end{bmatrix}\quad \mathbf{G}_v=\begin{bmatrix}0\\ \tau_{xy}\\ \tau_{yy}\\ u\tau_{xy}+v\tau_{yy}-q_y\end{bmatrix}.$$

In the above equations, each instantaneous variable is replaced by its mean and fluctuating part and then all equations are time averaged. Here the standard time average symbols are omitted for simplicity, and the following nondimensionalization is to be applied:

$$x=\frac{x^*}{H}\quad y=\frac{y^*}{H}\quad u=\frac{u^*}{a_\infty/\sqrt{\gamma}}\quad v=\frac{v^*}{a_\infty/\sqrt{\gamma}}$$

$$\rho=\frac{\rho^*}{\rho_\infty}\quad p=\frac{p^*}{p_\infty a_\infty^2/\gamma}\quad T=\frac{T^*}{T_\infty}\quad e_t=\frac{e_t^*}{a_\infty^2/\gamma}$$

$$q^r=\frac{q^{r*}}{\sigma T_\infty^4}\quad \mu=\frac{\mu^*}{\mu_\infty}\quad \lambda=\frac{\lambda^*}{\lambda_\infty}. \tag{3}$$

While the superscript * represents the real value,

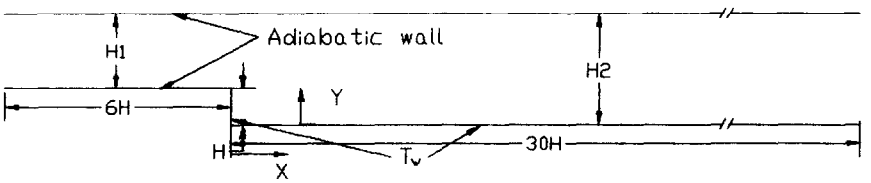

Fig. 1. Geometry for backward facing step flow.

the subscript ∞ represents the reference value. The speed of sound is denoted by $a = \sqrt{\gamma p/\rho}$.

The pressure is related to conservative flow variables $\tilde{Q}$ through the equation of state

$$p = \rho(\gamma-1)\{e_t - \tfrac{1}{2}(u^2+v^2)\}, \tag{4}$$

where γ is the ratio of specific heats.

The components of the viscous stress tensor τ_{ij} and heat flux q_i are, respectively, given by

$$\tau_{ij} = (\mu+\mu_t)\left(\frac{\partial u_i}{\partial x_j} + \frac{\partial u_j}{\partial x_i} + \tfrac{2}{3}\delta_{ij}\frac{\partial u_k}{\partial x_k}\right) \tag{5}$$

$$q_i = -(\lambda+\lambda_t)\frac{\partial T}{\partial x_i} + q_i^r. \tag{6}$$

Here μ_t, and λ_t are eddy viscosity and eddy thermal conductivity. The variation of μ, λ, C_p of air with temperature is as follows [7]:

$$\mu = \frac{14.58\times10^{-7}T^{3/2}}{110.4+T}\ \text{kg m}^{-1}\ \text{s}^{-1}$$

$$\lambda = \frac{2.6482\times10^{-3}T^{1/2}}{1+245.4\times10^{-12/T}/T}\ \text{W m}^{-1}\ \text{K}^{-1}$$

$$C_p = 0.917 + 2.58\times10^{-4}T - 3.98\times10^{-8}T^2\ \text{kJ kg}^{-1}\ \text{K}^{-1}. \tag{7}$$

The turbulent Prandtl number is set to 0.9 in order to find λ_t from μ_t.

2.2. *Radiative transfer equation*

The effect of radiation is taken into consideration in the energy conservation equation as the divergence of radiative heat flux, $-\nabla\cdot q^r$. For a gray medium, this term can be denoted by

$$-\nabla\cdot q^r = a(r)\left[\int_{4\pi} I(r,\Omega)\,d\Omega - 4\pi I_b\right], \tag{8}$$

where $I_b = \sigma T^4$.

To find the directional intensity $I(r,\Omega)$, the following radiative transfer equation (RTE) has to be solved:

$$(\Omega\cdot\nabla)I(r,\Omega) = -[a(r)+s(r)]I(r,\Omega) + a(r)I_b(r) + \frac{s(r)}{4\pi}\int_{4\pi} I(r,\Omega')\Phi(\Omega'\to\Omega)\,d\Omega'. \tag{9}$$

This equation shows that the rate of change of intensity in the direction of propagation, Ω, is attenuated by absorption and out-scattering (from direction Ω to Ω'), and is enhanced by emission and in-scattering (from direction Ω' to Ω).

In this study equation (9) is solved by using the discrete ordinates approximation [8] with $s = 0$. This is obtained by dividing the entire solid angle (4π steradians) into a finite number of ordinate directions with corresponding weight factors. The RTE is therefore written for each ordinate direction, while replacing the integral term by a quadrature summed over each ordinate. This method is sometimes referred to as the S_N approximation, where N represents the order of approximation (the number of discrete values of direction cosines to be considered). In general, for two-dimensional symmetric geometry, the total number of ordinate directions, M, is related to the order of the approximation, N, through the relationship $M = N(N+2)/2$. Preliminary evaluations revealed that the S_4 approximation is quite adequate in the present analysis, for no measurable gain in accuracy was obtained by higher order approximations.

For two-dimensional Cartesian coordinates, the RTE can be expressed for each individual ordinate direction, i, as

$$\xi_i\frac{\partial I_i}{\partial x} + \eta_i\frac{\partial I_i}{\partial y} + \beta I_i = aI_b + \frac{s}{4\pi}\sum_{j=1}^{M} w\Phi_{ij}I_j, \qquad i = 1,2,\ldots,M, \tag{10}$$

where the values i and j denote outgoing and incoming directions, respectively. ξ_i, η_i are the direction cosines of a discrete direction.

2.3. *Boundary and initial conditions*

(1) *Wall boundary conditions.* Along the walls, no-slip boundary condition ($u = 0, v = 0$) is specified. Whereas, the top wall is maintained adiabatic requiring the net heat flux by conduction and radiation to be zero, the step side wall and bottom wall behind the step are assigned constant temperature. The wall pressure is obtained using the boundary-layer assumption, such that its normal derivative vanishes at the wall. The wall emissivity (ε_w) is set to 0.8.

(2) *Subsonic inflow conditions.* The characteristic theory [9] allows three quantities to be specified. Here, the total pressure, total temperature, and flow angle have specified values at the inlet. The streamwise static pressure gradient is set to vanish at the inlet; i.e. $p_{1,j} = p_{2,j}$. From known values of the total pressure, static pressure and total temperature, the static temperature can be calculated from the following isentropic relation:

$$\frac{T_t}{T} = \left(\frac{p_t}{p}\right)^{(\gamma-1)/\gamma} \tag{11}$$

which then defines the speed of sound. Further, the Mach number can be calculated from

$$Ma = \sqrt{2\left\{\frac{(T_t/T)-1}{\gamma-1}\right\}} \tag{12}$$

which allows the calculation of the streamwise component of velocity by multiplying the Mach number by its sonic velocity. The transverse component of velocity can be estimated from the specified flow angle. The density and total internal energy can then be computed to complete the specification of all necessary conditions.

(3) *Subsonic outflow conditions.* The characteristic theory allows only one quantity to be specified at the outlet so that the static pressure is specified therein. The other flowfield quantities are computed using zero-order extrapolation from their upstream values.

3. NUMERICAL METHOD

In the present study, the LU-SSOR (lower–upper symmetric successive over relaxation) scheme is adopted to solve the two-dimensional Navier–Stokes equations. The LU-SSOR scheme employs implicit Newton iteration technique to solve the finite-volume approximation of the governing equations. The convergence of the Newton iteration method is assured by the diagonal dominance in the coefficient matrices generated by the LU-SSOR scheme. A detailed derivation of the LU-SSOR scheme can be found in the ref. [10]. The final discretized form of the equations can be given by

$$(D_\xi^- \mathbf{A}^+ + D_\eta^- \mathbf{B}^+ - \mathbf{A}^- - \mathbf{B}^-)(D_\xi^+ \mathbf{A}^- + D_\eta^+ \mathbf{B}^- + \mathbf{A}^+ + \mathbf{B}^+)\delta\tilde{\mathbf{Q}} = -(r_A + r_B)\{D_\xi(\tilde{\mathbf{F}}^n - \tilde{\mathbf{F}}_v^n) + D_\eta(\tilde{\mathbf{G}}^n - \tilde{\mathbf{G}}_v^n)\}, \quad (13)$$

where the Jacobian matrices **A**, **B** are defined as

$$\mathbf{A} = \frac{\partial \tilde{\mathbf{F}}}{\partial \tilde{\mathbf{Q}}}, \quad \mathbf{B} = \frac{\partial \tilde{\mathbf{G}}}{\partial \tilde{\mathbf{Q}}}. \quad (14)$$

In equation (13), D_ξ^- and D_η^- are backward difference operators, while D_ξ^+ and D_η^+ are forward difference operators. $\mathbf{A}^+$, $\mathbf{A}^-$, $\mathbf{B}^+$ and $\mathbf{B}^-$ are constructed such that the eigenvalues of '+' matrices become non-negative, whereas those of '−' matrices are kept non-positive, as follows

$$\mathbf{A}^\pm = \tfrac{1}{2}(\mathbf{A} \pm r_A I), \mathbf{B}^\pm = \tfrac{1}{2}(\mathbf{B} \pm r_B I), \quad (15)$$

where

$$r_A \geqslant \max(|\lambda_A|), \quad r_B \geqslant \max(|\lambda_B|).$$

Here, λ_A and λ_B represent the eigenvalues of Jacobian matrices. After expanding out the difference operators on the left hand side (LHS), equation (13) becomes

$$\{(r_A + r_B)I - \tilde{\mathbf{A}}_{i-1,j}^+ - \tilde{\mathbf{B}}_{i,j-1}^+\}\{(r_A + r_B)I + \tilde{\mathbf{A}}_{i+1,j}^- + \tilde{\mathbf{B}}_{i,j+1}^-\}\delta\tilde{\mathbf{Q}}_{i,j} = -(r_A + r_B)\{D_\xi(\tilde{\mathbf{F}}^n - \tilde{\mathbf{F}}_v^n) + D_\eta(\tilde{\mathbf{G}}^n - \tilde{\mathbf{G}}_v^n)\}. \quad (16)$$

The present numerical method eliminates the need for banded block matrix inversions without using a diagonalization procedure. In fact, with a forward diagonal sweep for the inversion of the first operator and a backward diagonal sweep for the inversion of the second operator only scalar diagonal inversions are needed to solve equation (16).

In order to take account of turbulent flow, the zero-equation algebraic turbulence model developed by Baldwin and Lomax [11] is used. This model is a two-layer model in which an eddy viscosity is calculated at both the inner and outer regions. In both regions, the distribution of vorticity is used to determine the length scales. The primary advantage of this model is its simplicity, so that the boundary layer thickness does not need to be calculated.

4. RESULTS AND DISCUSSION

In order to verify the present compressible Navier–Stokes code, the internal static pressure is calculated for JPL nozzle and compared with the experimental data [12] as shown in Fig. 2. The inflow stagnation pressure and stagnation temperature are 4.824×10^6 Pa and 300 K, respectively. The supersonic outflow conditions are given. The present results are in good agreement with the experimental data.

After validating the computational code as above, the compressible turbulent flow over the backward facing step is computed and the results are cast in the following. The grid system is depicted in Fig. 3, in which 120 by 60 mesh points are placed along the

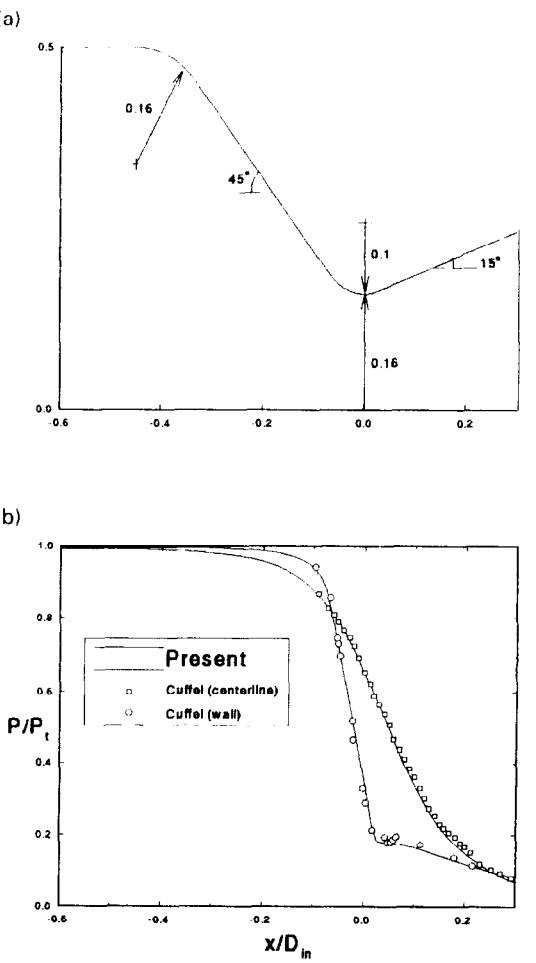

Fig. 2. JPL nozzle geometry and its pressure distribution on the wall and centerline. (a) JPL nozzle geometry. (b) Pressure distribution on the wall and centerline.

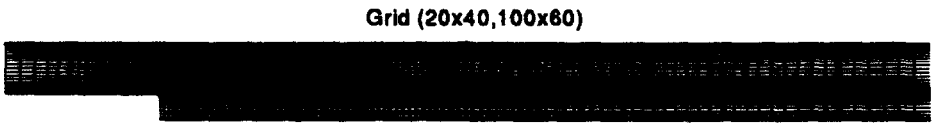

Fig. 3. Grid system for backward facing step flow.

streamwise and transverse directions. More grids are laid out near the wall and step. The total pressure and total temperature of inlet flow are 1.042×10^5 Pa and 712.6 K, respectively. The outflow static pressure is set to be 1.013×10^5 Pa. These conditions correspond to inlet Ma number of 0.3 and inlet Reynolds number of 8.421×10^4 [13]. The inflow is assumed to be fully developed turbulent flow.

The streamlines are plotted for various thermal conditions in Fig. 4(a–e): (a) all the walls are adiabatic while neglecting radiation; (b) the thermal condition at the step wall and the bottom wall behind the step is changed to 2000 K, while still neglecting radiation; (c–e) the thermal condition at the walls are the same as in the case (b). However, the radiation effect is taken into consideration with absorption coefficient $a = 10, 20, 40\ \mathrm{m}^{-1}$, respectively.

In the case (a) the reattachment length is observed to be about $6.9H$, which is considered to be consistent with former results ($4.9H < x_R < 8.2H$) [14]. In this case all the fluid temperature is uniformly kept at the same temperature as inlet, since all the walls are adiabatic. When the adiabatic lower walls are replaced by the constant wall temperatures with 2000 K, which corresponds to case (b), the reattachment length becomes shorter than case (a). In this case, the fluid temperature increases due to heat addition from the lower walls as shown in Fig. 5(b), representing the isothermal contours so that the static pressure is also increased. However, since the outflow static pressure is set at a constant value, the adverse pressure gradient in case (b) becomes smaller than that in case (a). The fundamental mechanism to determine the reattachment point is known to be reentrainment of the shear layer [15]. That is, the flow reattaches when the pressure-gradient-driven backflow balances with the entrained flow from the recirculating zone to the shear layer. When the adverse pressure gradient is reduced, less fluid is coming back into the recirculating zone, so that the shear layer requires a shorter length to entrain the backflow outward. That is why the decrease in the adverse pressure gradient leads to the decrease in reattachment length such that case (b) has a shorter reattachment length. The reattachment

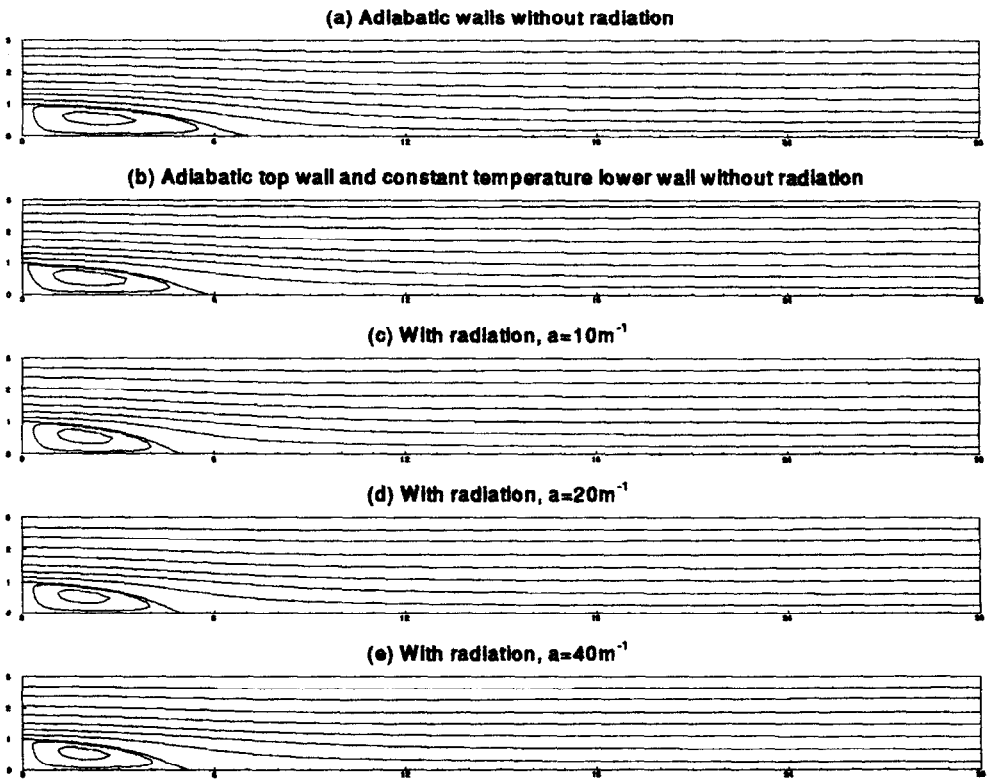

Fig. 4. Streamlines for various thermal conditions.

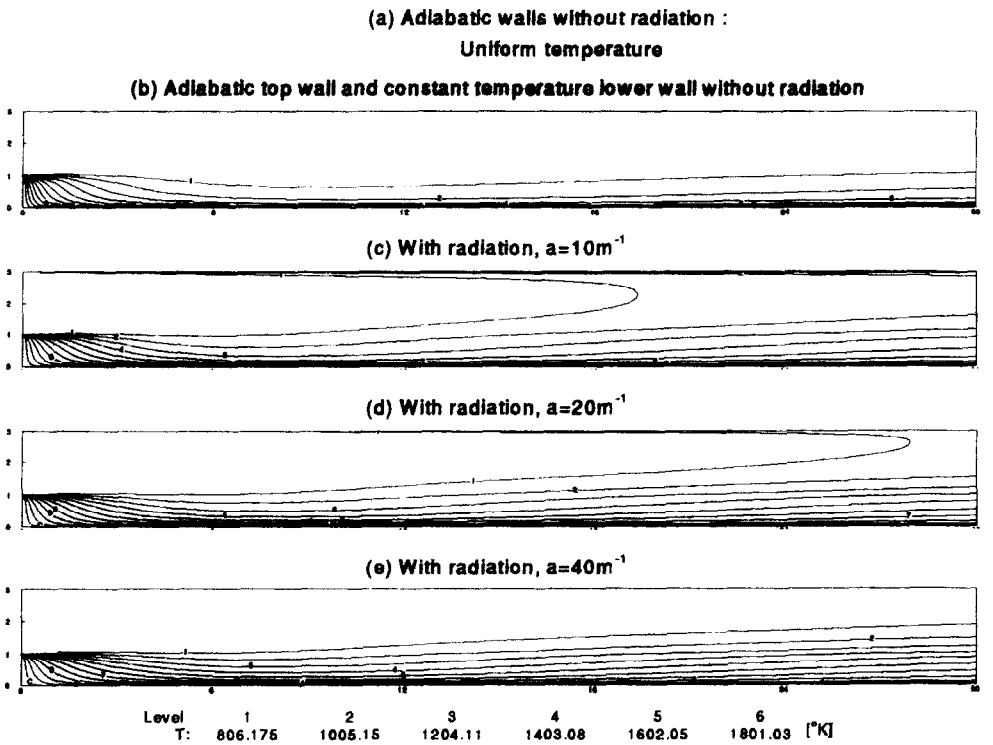

Fig. 5. Temperature contours for various thermal conditions.

length is also linked to the shear-layer growth rate. When the shear-layer growth rate is increased, the entrainment rate from the recirculation zone also increases. The shear layer, therefore, comes to require a shorter reattachment length to entrain outward the fluid coming back from the reattachment zone.

Once the radiation effect is introduced as in the cases (c–e), as seen in Fig. 5, the fluid temperature is increased further due to greater radiative energy absorption from the lower wall than case (b). The consequent smaller adverse pressure gradients obtained in cases (c–e), thus, produce an even shorter reattachment length than case (b). Therefore, the turbulent boundary layer after reattachment is more quickly developed. In Fig. 5(c–e) it is also observed that the fluid can warm up increasingly fast through the far-reaching effects of radiation from the lower walls, as the absorption coefficient decreases.

The pressure contours are depicted in Fig. 6. After a sudden expansion, the velocity is reduced while the pressure is minimum at the step and then increases along the duct in case (a). In cases (b–e), as the fluid is heated up, the pressure is increased further and the points of maximum pressures occur in the middle of the duct. Afterwards, along the downstream, the pressure is observed to decrease again so that the fluid is accelerated again as shown in Fig. 7, in which the axial velocity variation is shown at five locations for $a = 10\ \mathrm{m}^{-1}$. In case (c), the maximum pressure region is located upstream, compared with case (e), because the fluid is warmed up faster as a result of a smaller absorption coefficient, as can be seen in Fig. 6.

The effect of radiation on the temperature distribution is shown in Fig. 8 at two axial locations $x = 5H$, $25H$ from the step. For the case of no radiation, the fluid temperature steadily decreases from the lower hot wall toward the top adiabatic wall. For the case with radiation, the bigger the absorption coefficient, the higher the fluid temperature is near the lower hot wall, but the lower the fluid temperature is near the top adiabatic wall. The reason is that the radiation has a far-reaching effect as the absorption coefficient decreases. It must also be noted that there exists a temperature gradient at the top adiabatic wall for the case with radiation, because it is adiabatic from the sense of total heat flux comprising conduction and radiation.

The conductive, convective, radiative and total heat flux vectors are plotted for $a = 10\ \mathrm{m}^{-1}$ in Fig. 9. The recirculating zone is especially emphasized, for the convective heat flux is predominant elsewhere due to its high fluid velocity. It is only in the recirculating zone that the radiative heat flux becomes comparable to the convective heat flux. Nevertheless, in the recirculating zone, the role of conduction is almost negligible. In the given figure the maximum radiative heat flux amounts to only 6% of the maximum convective heat flux. Therefore, the effect of radiation would be quite limited in this kind of physical condition chosen for this study.

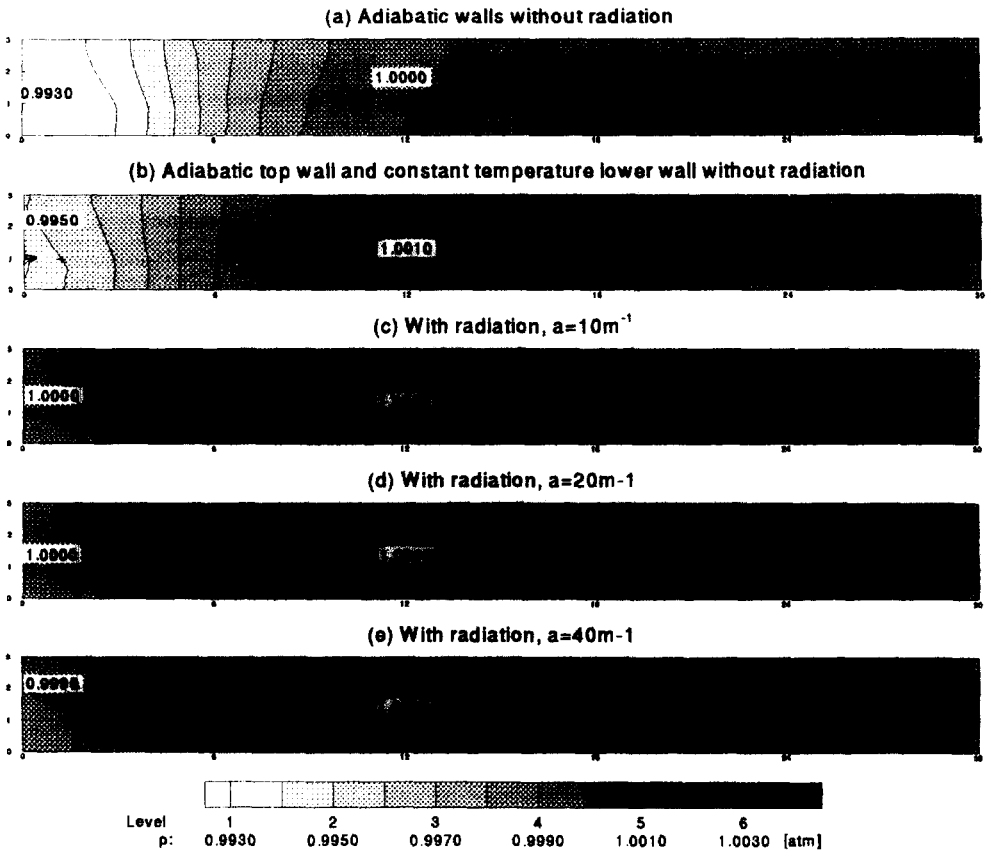

Fig. 6. Pressure contours for various thermal conditions.

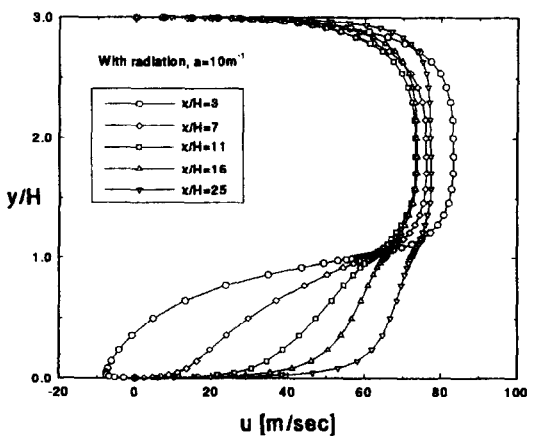

Fig. 7. Axial velocity variation along the downstream.

5. CONCLUSION

Numerical analysis has been performed to analyze a compressible turbulent flow over a backward facing step. Especially, the effect of radiation on the thermo-fluid dynamic behavior has been discussed. It led to a decrease in the reattachment length due to faster heating, which results in the lower adverse pressure gradient. Temperature distribution was also influenced by radiation, depending on the absorption coefficient. But the radiative heat flux was found to be negligible except for the recirculating region, compared with the convective heat flux. Consequently, the role of radiation is considered to be quite limited in this sense for the conditions given here.

Acknowledgements—The authors are grateful for the financial support by ADD (Agency for Defense Development) under contract ATRC-421-940903.

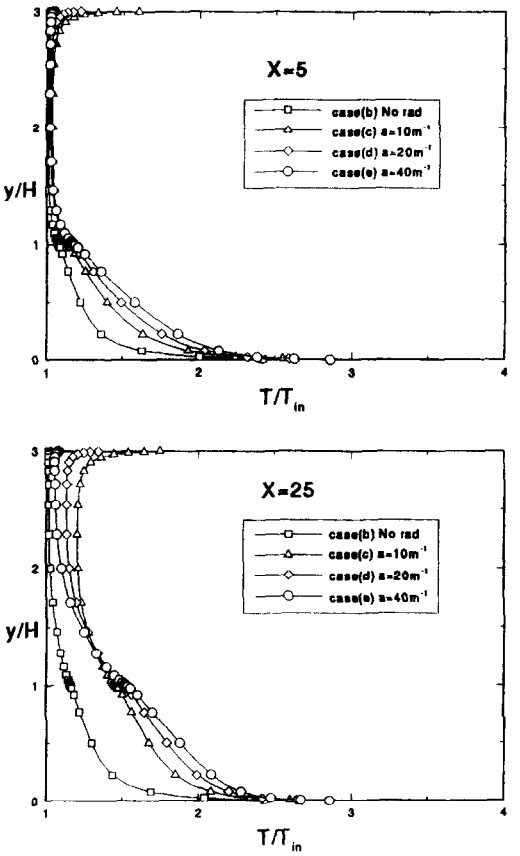

Fig. 8. Temperature variation along the transverse direction for various thermal conditions.

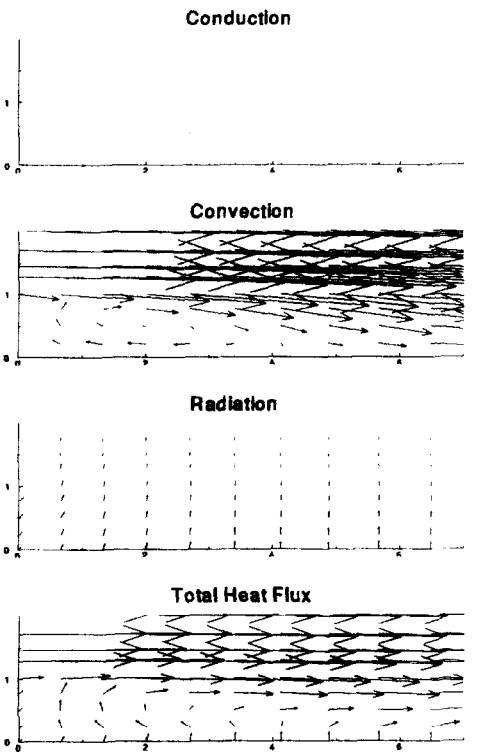

Fig. 9. Heat flux vectors (with radiation, $a = 10\ \mathrm{m}^{-1}$).

REFERENCES

1. M. Kobiyama, H. Taniguchi and T. Saito, The numerical analysis of heat transfer combined with radiation and convection. *Bull. JSME* **22**, 707–714 (1979).
2. T. K. Kim and H. S. Lee, Two-dimensional anisotropic scattering radiation in a thermally developing poiseuille flow. *J. Thermophys. Heat Transfer* **4**, 292–298 (1990).
3. R. Echigo, S. Hasegawa and K. Kamiuto, Composite heat transfer in a pipe with thermal radiation of two-dimensional propagation—in connection with the temperature rise in flowing medium upstream from heating section. *Int. J. Heat Transfer* **18**, 1149–1159 (1975).
4. T. F. Smith, K. H. Byun and M. J. Ford, Heat transfer for flow of an absorbing, emitting, and isotropically scattering medium through a tube with reflecting walls. *Proceedings of the Eighth International Heat-Transfer Conference*, Vol. 2, pp. 803–808 (1986).
5. J. C. Chai, H. S. Lee and S. V. Patankar, Laminar heat transfer of a radiating fluid in a backward facing step flow. *Proceedings of Transport Phenomean in Thermal Engineering Conference*, pp. 209–214 (1993).
6. G. Schulte, Fuel regression and flame stabilization studies of solid-fuel ramjets. *J. Propulsion Power* **2**, 301–304 (1986).
7. S. Ostrach, Natural convection in enclosure. In *Advances in Heat Transfer*, Vol. 8, p. 161–227. Academic Press, New York (1972).
8. M. F. Modest, *Radiative Heat Transfer*, p. 541. McGraw-Hill, New York (1993).
9. K. A. Hoffmann and S. T. Chiang, *Computational Fluid Dynamics for Engineers* Vol. II, p. 103. Engineering Education System, Kansas (1993).
10. S. Yoon and A. Jameson, Lower–upper symmetric-Guass–Seidel method for the Euler and Navier–Stokes equations. *AIAA J.* **26**, 1025–1027 (1988).
11. B. Baldwin and H. Lomax, Thin layer approximation and algebraic model for separated turbulent flows. AIAA Paper 78–257 (1978).
12. R. F. Cuffel, L. H. Back and P. F. Massier, Transonic flow field in a supersonic nozzle with small throat radius of curvature. *AIAA J.* **7**, 1364–1365. (1969).
13. W. G. Habashi, *Advances in Computational Transonics*, p. 491. Pineridge Press, Swansea (1985).
14. J. K. Eaton and J. P. Johnston, Review of research on subsonic turbulent flow reattachment. *AIAA J.* **19**, 1093–1100 (1981).
15. J. K. Eaton and J. P. Johnston, Turbulent flow reattachment: an experimental study of the flow and structure behind a backward-facing step, Report MD-39, Thermosciences Division, Department of Mechanical Engineering, Stanford University (1980).